Astronomy & Astrophysics manuscript no. 14266
April 13, 2010

Absolute dimensions of eclipsing binaries. XXVIII. ⋆

BK Pegasi and other F-type binaries: Prospects for calibration of convective core overshoot ⋆⋆

J.V. Clausen[1], S. Frandsen[2], H. Bruntt[3,4], E. H. Olsen[1], B. E. Helt[1], K. Gregersen[1], D. Juncher[1], and P. Krogstrup[1]

[1] Niels Bohr Institute, Copenhagen University, Juliane Maries Vej 30, DK-2100 Copenhagen Ø, Denmark
[2] Department of Physics and Astronomy, University of Aarhus, Ny Munkegade, DK-8000 Aarhus C, Denmark
[3] Observatoire de Paris, LESIA, 5 Place Jules Janssen, 95195 Meudon, France
[4] Sydney Institute for Astronomy, School of Physics, University of Sydney, NSW 2006, Australia

Received 16 February 2010 / Accepted 26 March 2010

ABSTRACT

Context. Double-lined, detached eclipsing binaries are our main source for accurate stellar masses and radii. In this paper we focus on the 1.15–1.70 $M_\odot$ interval where convective core overshoot is gradually ramped up in theoretical evolutionary models.

Aims. We aim to determine absolute dimensions and abundances for the F-type detached eclipsing binary BK Peg, and to perform a detailed comparison with results from recent stellar evolutionary models, including a sample of previously studied systems with accurate parameters.

Methods. *uvby* light curves and $uvby\beta$ standard photometry were obtained with the Strömgren Automatic Telescope, ESO, La Silla, and high-resolution spectra were acquired with the FIES spectrograph at the Nordic Optical Telescope, La Palma.

Results. The $5\overset{\mathrm{d}}{.}49$ period orbit of BK Peg is slightly eccentric ($e = 0.053$). The two components are quite different with masses and radii of (1.414 ± 0.007 $M_\odot$, 1.988 ± 0.008 $R_\odot$) and (1.257 ± 0.005 $M_\odot$, 1.474 ± 0.017 $R_\odot$), respectively. The measured rotational velocities are 16.6 ± 0.2 (primary) and 13.4 ± 0.2 (secondary) km s^{-1}. For the secondary component this corresponds to (pseudo)synchronous rotation, whereas the primary component seems to rotate at a slightly lower rate. We derive an iron abundance of [Fe/H] $= -0.12 \pm 0.07$ and similar abundances for Si, Ca, Sc, Ti, Cr and Ni. The stars have evolved to the upper half of the main-sequence band. Yonsei-Yale and Victoria-Regina evolutionary models for the observed metal abundance reproduce BK Peg at ages of 2.75 and 2.50 Gyr, respectively, but tend to predict a lower age for the more massive primary component than for the secondary. We find the same age trend for three other upper main-sequence systems in a sample of well studied eclipsing binaries with components in the 1.15–1.70 $M_\odot$ range. We also find that the Yonsei-Yale models systematically predict higher ages than the Victoria-Regina models. The sample includes BW Aqr, and as a supplement we have determined a [Fe/H] abundance of -0.07 ± 0.11 for this late F-type binary.

Conclusions. We propose to use BK Peg, BW Aqr, and other well-studied 1.15–1.70 $M_\odot$ eclipsing binaries to fine-tune convective core overshoot, diffusion, and possibly other ingredients of modern theoretical evolutionary models.

Key words. Stars: evolution – Stars: fundamental parameters – Stars: binaries: eclipsing – Stars: individual: BK Peg, BW Aqr – Techniques: photometric – Techniques: spectroscopic

1. Introduction

Detached, double-lined eclipsing binaries (dEB) are our main source for stellar masses and radii, today accurate to 1% or better (Torres et al. 2009), and they also provide stringent tests of various aspects of stellar evolutionary models. For this purpose, well-established abundance information is needed, as demonstrated by e.g. Clausen et al. (2008b, hereafter CTB08). One of the troublesome ingredients in theoretical models for stars heavier than the Sun is the amount of and treatment of convective core overshoot, and in this paper we focus on that aspect.

The literature on the existence and calibration of core overshoot is extensive, and here we only draw attention to a few studies based on binary and cluster results. From a sample of 1.5–2.5 $M_\odot$ dEBs and turn-off stars in IC 4651 and NGC 2680, Andersen et al. (1990) found strong evidence for convective overshoot in intermediate-mass stars. Clausen (1991) found indication for core overshoot for the 1.4+1.5 $M_\odot$ late-F type dEB BW Aqr and discussed BK Peg as well, and recently, Lacy et al. (2008) found that for the 1.5 $M_\odot$ F7 V system GX Gem, the lowest core overshoot parameter $\alpha_{\rm ov}$ consistent with observations is approximately

Send offprint requests to: J.V. Clausen,
e-mail: jvc@nbi.ku.dk

⋆ Based on observations carried out at the Strömgren Automatic Telescope (SAT) and the 1.5m telescope (63.H-0080) at ESO, La Silla, and the Nordic Optical Telescope at La Palma

⋆⋆ Tables 13–17 are available in electronic form at the CDS via anonymous ftp to cdsarc.u-strasbg.fr (130.79.128.5) or via http://cdsweb.u-strasbg.fr/cgi-bin/qcat?J/A+A/

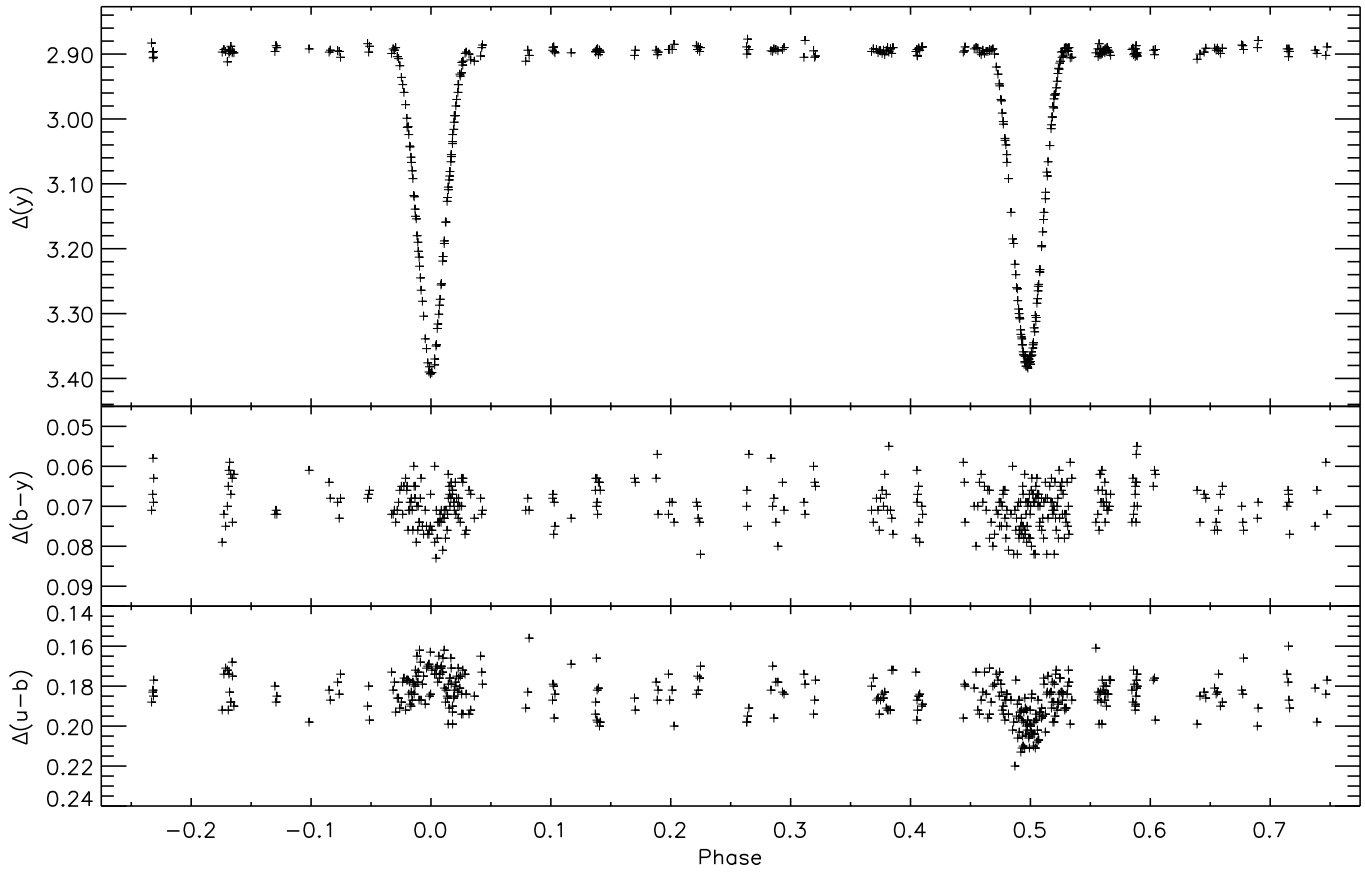

Fig. 1. y light curve and $b-y$ and $u-b$ colour curves (instrumental system) for BK Peg.

0.18 (in units of the pressure scale height). The question of mass-dependence of the degree of core overshoot has – again based on dEB samples – been addressed by e.g. Ribas et al. (2000) and Claret (2007), but they arrive at very different conclusions.

Most recent grids of stellar evolutionary calculations include core overshoot, but the recipes in terms of mass and abundance dependence are somewhat different. We refer to Sect. 9 for details.

Our main motivation to undertake a study of BK Peg has been that a) it has evolved to the upper part of the main-sequence band and is therefore well-suited for core overshoot tests, but published dimensions are not of sufficient quality, and b) few similar well-studied systems are known. Below we present absolute dimensions and abundances based on new *uvby* light curves and high-resolution spectra and compare BK Peg and other similar systems with Yonsei-Yale and Victoria-Regina stellar evolutionary models.

In Appendix A we present a spectroscopic abundance analysis for BW Aqr as supplement to the study of this binary by Clausen (1991).

2. BK Peg

BK Peg (BD +25 5003, m_V = 9.98, Sp. type F8, P = $5\overset{\mathrm{d}}{.}49$), is a well detached, double-lined eclipsing binary with 1.41 and 1.26 $M_\odot$ components in a slightly eccentric (e = 0.0053) orbit. It is unusual in the sense that the more massive, larger, and more luminous component is slightly cooler than the other component. This is due to evolution, where the more massive component has evolved to the upper part of the main-sequence band.

The eclipsing nature of BK Peg was discovered by Hoffmeister (1931), and Lause (1935, 1937) visually observed several times of minima. Popper & Dumont (1977) obtained BV light curves at the Palomar and Kitt Peak observatories, which were later analysed by Popper & Etzel (1981). Preliminary absolute dimensions were included by Popper in his critical review of stellar masses (Popper 1980), and soon after he presented spectroscopic elements and improved absolute dimensions (Popper 1983). He reached component masses accurate to about 1% and radii accurate to 4% (primary) and 7% (secondary). Demircan et al. (1994) presented photoelectric UBV light curves and an improved ephemeris, as well as absolute dimensions, which, within the uncertainties, agree with those by Popper; see also Popper & Etzel (1995) for clarification on terminology. We refer to the more massive, larger but cooler component as the primary (p) component, which, for the ephemeris we adopt (Eq. 1), is eclipsed at phase 0.0.

3. Photometry

Below, we present the new photometric material for BK Peg and refer to Clausen et al. (2001; hereafter CHO01) for

Table 1. Photometric data for BK Peg and the comparison stars.

Object	Sp. Type	Ref.	V	σ	$b-y$	σ	m_1	σ	c_1	σ	N($uvby$)	β	σ	N(β)
BK Peg	F8[a]	C10	9.982	7	0.362	6	0.143	12	0.456	12	176	2.639	7	9
		C10	10.463	4	0.369	7	0.136	11	0.477	4	6			
HD222249	F5 IV[b]	C10	7.146	6	0.309	4	0.177	8	0.503	8	118	2.645	3	8
		O83	7.139	5	0.317	3	0.158	4	0.503	4	1			
		O94	7.151	9	0.317	3	0.161	3	0.507	2	3	2.645	8	3
		P69	7.010		0.303		0.190		0.487		2			
HD222391	G0 III[c]	C10	7.566	6	0.362	6	0.185	11	0.424	8	134	2.617	4	8
		O83	7.559	5	0.371	3	0.170	4	0.420	5	1			
		O94			0.372	3	0.167	4	0.427	6	1	2.620	6	2
HD223323	F2 IV-V[d]	C10	7.084	6	0.290	5	0.138	10	0.414	9	189	2.636	7	13
		J96	7.076	4	0.302	1	0.123	1	0.407	1	9	2.640		
		J96	7.094	2	0.300	0	0.128	5	0.409	4	2			
		J96	7.089	1	0.299	0	0.120	0	0.406	1	2			
		O83	7.080	6	0.296	5	0.124	5	0.412	4	4	2.643	5	4

[a] Popper (1983), [b] Harlan & Taylor (1970), [c] Heard (1956), [d] Harlan (1969)

NOTE 1: References are: C10 = This paper. J96 = Jordi et al. (1996). O83 = Olsen (1983). O94 = Olsen (1994). P69 = Perry (1969).
NOTE 2: For BK Peg, the $uvby\beta$ information by C10 is the mean value outside eclipses (first line) and during the central part of secondary eclipse (second line), where 98% (y) of the light of the secondary component is eclipsed.
NOTE 3: N is the total number of observations used to form the mean values, and σ is the rms error (per observation) in mmag.

further details on observation and reduction procedures, and determination of times of minima.

3.1. Light curves for BK Peg

The differential $uvby$ light curves of BK Peg were observed at the Strömgren Automatic Telescope (SAT) at ESO, La Silla with its 6-channel $uvby\beta$ photometer on 66 nights between October 2000 and September 2003 (JD2451828–2452910). They contain 384 points per band with most phases covered at least twice. The observations were done through an 18 arcsec diameter circular diaphragm at airmasses between 1.8 and 2.2. HD 222249, HD 222391, and HD 223323 – all within a few degrees of BK Peg on the sky – were used as comparison stars and were all found to be constant within a few mmag; see Table 1. The light curves are calculated relative to HD 223323, but all comparison star observations were used, shifting them first to the same light level. HD 223323 has later been found to be a double-lined spectroscopic binary with an estimated orbital inclination of about 63°; the orbital period is 1175 days and the orbital eccentricity is 0.6 (Griffin 2007). The average accuracy per light curve point is about 5 mmag (ybv) and 8 mmag (u). The light curves (Table 13) will only be available in electronic form.

As seen from Fig. 1, BK Peg is well detached with nearly identical eclipse depths of about 0.5 mag. In the y, b, and v bands, the primary eclipse at phase 0.0, which is a transit, is slightly deeper than the secondary eclipse (almost total occultation), which occurs at phase 0.4976. In the u band the secondary eclipse is, however, the slightly deeper one.

3.2. Standard photometry for BK Peg

Standard $uvby\beta$ indices for BK Peg and the three comparison stars, observed and derived as described by CHO01, are presented in Table 1. As seen, the indices are based on many observations and their precision is high. For comparison, we have included published photometry from other sources. In general, the agreement is good, but in some cases differences are larger than the quoted errors; we have used the new results for the analysis of BK Peg.

3.3. Times of minima and ephemeris for BK Peg

Three times of secondary minimum, but none of primary, have been determined from the $uvby$ light curve observations. They are listed in Table 2 together with available measured times. From separate weighted least squares fit to the times of primary and secondary minima, respectively, we derive the linear ephemeris given in Eq. 1.

$$\begin{array}{rcrcrcl} \text{Min I} = & & 2450706.46968 & + & 5\overset{\text{d}}{.}48991046 & \times E & \\ & & \pm 38 & & \pm 56 & & \end{array} \quad (1)$$

Within errors, the two types of minima yield identical periods, and the new ephemeris is in good agreement with that by Demircan et al. (1994); see also Kreiner et al. (2001) and Kreiner (2004)[1].

4. Spectroscopy

In order to perform abundance determinations and also improve the spectroscopic elements by Popper (1983), we have obtained 13 high-resolution (R = 45000) spectra with the FIES fibre echelle spectrograph at Nordic Optical Telescope, La Palma during five consecutive nights in August 2007; see Table 3. For the basic reduction of the spectra, we have applied the IRAF based FIEStool package[2]. Subsequently, dedicated IDL[3] programs were applied

[1] `http://www.as.ap.krakow.pl/ephem`
[2] see `http://www.not.iac.es` for details on FIES and FIEStool.
[3] `http://www.ittvis.com/idl/index.asp`

Table 2. Times of primary (P) and secondary (S) minima for BK Peg.

HJD − 2 400 000	rms publ.	rms adopt.	(O-C)/phase[a] days	Type	Observing method[b]	Reference[c]
2426600.280	0.005		0.0072	P	V	D77
2427418.270		0.01	0.0005	P	V	L35
2427429.277		0.01	0.0277	P	V	-
2427698.252		0.01	−0.0029	P	V	-
2427709.224		0.01	−0.0108	P	V	-
2427764.158		0.01	0.0241	P	V	-
2428373.507		0.01	−0.0069	P	V	L37
2428395.473		0.01	−0.0006	P	V	-
2428428.424		0.01	0.0110	P	V	-
2428461.348		0.01	−0.0045	P	V	-
2428538.220		0.01	0.0088	P	V	-
2441587.7265	0.0010		−0.0019	P	PE	P83
2446737.244		0.01	−0.0204	P	V	B87
2448900.28902	0.00056		−0.00012	P	PE	D94
2450706.4701	0.0003		0.0004	P	PE	A03
2451052.3325	0.0007		−0.0015	P	PE	-
2454000.4181	0.0028		0.0021	P	CCD	H07
2427684.556		0.01	0.5047	S	V	L35
2427717.444		0.01	0.4953	S	V	-
2427739.416		0.01	0.4975	S	V	-
2427827.250		0.01	0.4968	S	V	-
2428480.560		0.01	0.4987	S	V	L37
2428513.497		0.01	0.4982	S	V	-
2428535.438		0.01	0.4949	S	V	-
2428546.449		0.01	0.5005	S	V	-
2428557.427		0.01	0.5002	S	V	-
2428579.368		0.01	0.4968	S	V	-
2441974.7539	0.0003		0.4976	S	PE	P83
2443786.43575	0.00025	0.00100	0.49967	S	PE	D94
2448886.56089	0.00100		0.49937	S	PE	-
2450319.4175	0.0004		0.4975	S	PE	A03
2451137.4160	0.0004		0.4979	S	PE	-
2451845.6124	0.0002		0.4975	S	PE	C10
2451867.5715	0.0008		0.4974	S	PE	-
2452136.580	0.002		0.4979	S	CCD	D01
2452910.6565	0.0002		0.4978	S	PE	C10

[a] O-C values (P) and phases (S) are calculated for the ephemeris given in Eq. 1.
[b] Observing methods are: V = visual; PE = photoelectric; CCD = CCD.
[c] References are: A03 = Ak et al. (2003). B87 = Braune & Hübscher (1987). C10 = This paper. D77 = Dworak (1977). D94 = Demircan et al. (1994). D01 = Diethelm (2001). H07 = Hübscher & Walter (2007). L35 = Lause (1935). L37 = Lause (1937). P83 = Popper & Dumont (1977), redetermined.

to remove cosmic ray events and other defects, and for normalisation of the individual orders. For each order, only the central part with acceptable signal-to-noise ratios was kept for further analysis.

The radial velocities for BK Peg were measured from 40 useful orders of the 13 FIES spectra. We applied the broadening function (BF) formalism (Rucinski 1999, 2002, 2004), using $v \sin i = 0$ synthetic templates matching the effective temperature, $\log(g)$, and metal abundance of the components of BK Peg. They were calculated with the *bssynth* tool, which applies the SYNTH software (Valenti & Piskunov 1996) and modified ATLAS9 models (Heiter et al. 2002). Since the components have nearly identical temperatures, the two templates are very similar and lead to practically identical results. As described by e.g. Kaluzny et al. (2006), the projected rotational velocities $v \sin i$ of the components and (monochromatic) light/luminosity ratios between them can also be obtained from analyses of the BFs.

For each spectrum, BFs were calculated for each of the selected orders, and a mean BF was then calculated together with weights for each order based on the root mean square deviation of the individual BFs from the mean BF. The final BF is the weighted average for the selected orders. The radial velocites, the $v \sin i$'s, and the light ratio were derived by fitting a rotational profile for both stellar components, convolved with a Doppler profile corresponding to the instrumental resolution, to the final BF for each observed spectrum.

The radial velocities are listed in Table 4. The final values of $v \sin i$ and light ratio were calculated as the mean values for the 13 spectra, with errors estimated from the deviations from spectrum to spectrum. For the primary and secondary components of BK Peg, we obtain mean rotational velocities of 16.6 ± 0.2 and 13.4 ± 0.2 km s^{-1}, respectively. For the light ratio we find $L_s/L_p = 0.57 \pm 0.02$.

In addition, we have determined the light ratio between the components by directly comparing the FIES spectra

Table 3. Log of the FIES observations of BK Peg.

HJD−2 400 000[a]	phase	t_{exp}[b]	S/N[c]
54333.45954	0.6647	300	60
54333.46395	0.6655	300	55
54334.42028	0.8397	300	20
54335.52799	0.0414	300	70
54335.53872	0.0434	600	85
54335.62203	0.0586	600	85
54335.72881	0.0780	600	100
54336.41869	0.2037	600	55
54336.43503	0.2067	600	60
54336.52436	0.2229	600	75
54336.74168	0.2625	600	80
54337.44772	0.3911	600	65
54337.58944	0.4169	600	75

[a] Refers to mid-exposure
[b] Exposure time in seconds
[c] Signal-to-noise ratio measured around 6070 Å

Table 4. Radial velocities of BK Peg and residuals from the final spectroscopic orbit presented in Table 8.

HJD −2 400 000	Phase	RV_p km s^{-1}	RV_s km s^{-1}	$(O-C)_p$ km s^{-1}	$(O-C)_s$ km s^{-1}
54333.45954	0.6647	60.398	−83.802	0.25	0.28
54333.46395	0.6655	60.694	−83.936	0.35	0.38
54334.42028	0.8397	58.578	−81.562	−0.50	0.09
54335.52799	0.0414	−28.144	15.916	−0.19	−0.38
54335.53872	0.0434	−28.875	16.995	0.02	−0.33
54335.62203	0.0586	−36.037	24.823	0.05	−0.42
54335.72881	0.0780	−44.698	34.832	0.22	−0.10
54336.41869	0.2037	−83.237	77.803	0.15	0.44
54336.43503	0.2067	−83.671	78.279	0.11	0.47
54336.52436	0.2229	−85.447	80.223	0.03	0.45
54336.74168	0.2625	−86.151	81.269	−0.01	0.50
54337.44772	0.3911	−56.696	48.134	−0.20	−0.59
54337.58944	0.4169	−46.161	36.119	−0.28	−0.80

and synthetic binary spectra, calculated for a range of luminosity ratios between the components. Adopting the temperatures, surface gravities, rotational velocities, and metallicities listed in Table 10, and using several spectral orders covering 5300–5800 Å, we obtain the best line fits for a light ratio of 0.57 ± 0.04. As expected, since the components have nearly identical temperatures, we find no significant wavelength dependence of the spectroscopic light ratio, even if a broader wavelength region is used.

5. Photometric elements

Since BK Peg is well-detached, the photometric elements have been determined from JKTEBOP[4] analyses (Southworth et al. 2004a,2004b) of the *uvby* light curves. The underlying simple Nelson-Davis-Etzel binary model (Nelson & Davis 1972, Etzel 1981, Popper & Etzel 1981, Martynov 1973) represents the deformed stars as biaxial ellipsoids and applies a simple bolometric reflection model. We refer to CTB08 for details on the general approach applied. In tables and text, we use the following symbols: i orbital inclination; e eccentricity of orbit; ω longitude of periastron; r relative radius; $k = r_s/r_p$; u linear limb darkening coefficient; y gravity darkening coefficient; J central surface brightness; L luminosity; $T_{\rm eff}$ effective temperature.

The mass ratio between the components was kept at the spectroscopic value, see Sect. 6. The simple built-in bolometric reflection model was used, linear limb darkening coefficients by Van Hamme (1993) and Claret (2000) were applied, and gravity darkening coefficients corresponding to radiative atmospheres were adopted. Identical coefficients were used for the two components, since their effective temperatures and surface gravities are sufficiently identical. Effective temperatures determined from the standard *uvby* and JHK_s indices outside eclipses are listed in Table 5. As seen, the results from the different calibrations agree well; we have adopted the temperature based on the Holmberg et al. (2007) calibration.

Solutions for BK Peg, based on Van Hamme limb darkening coefficients, are presented in Table 6, and $O-C$ residuals of the y observations from the theoretical light curve are shown in Fig. 2. As seen, the results from the four bands agree well. Changing to Claret (2000) limb darkening coefficients, which are 0.07–0.09 higher, increases the radius of the primary component by only 0.4%, whereas that of the secondary component is increased by 1.5%. This is linked to a 1% larger k and a 29% smaller $e\sin(\omega)$, reducing e by 10%. Limb darkening coefficients determined from the light curves reproduce those by Van Hamme better than those by Claret, but have uncertainties of about ±0.12. Including non-linear limb darkening (logarithmic or square-root law) has no significant effect on the photometric elements.

The adopted photometric elements listed in Table 7 are the weighted mean values of the JKTEBOP solutions adopting the linear limb darkening coefficients by Van Hamme. Realistic errors, based on 10 000 Monte Carlo simulations in each band and on comparison between the *uvby* solutions, have been assigned. The Monte Carlo simulations include random variations within ±0.07 of the linear limb darkening coefficients. As seen, r_p becomes more accurate than r_s. This is because it correlates less with k, probably related to the secondary eclipse being nearly total for the adopted elements. It should be noted that the *ybv* luminosity ratios from the light curve solutions agree very well with the spectroscopic light ratio (Sect. 4).

For comparison, Popper & Etzel (1981) obtained $r_p = 0.108 \pm 0.04$ and $r_s = 0.086 \pm 0.006$, assuming $e\sin(\omega) = 0$ and adopting $k = 0.80 \pm 0.05$ in order to reproduce a mean ratio of 0.69 ± 0.03 between selected secondary and primary lines, measured on photographic spectra. This ratio is, however, much higher than the light ratio we derive from the FIES spectra, leading to a higher k. Popper & Etzel also obtain a somewhat larger value for $r_p + r_s$. The relative radii presented by Demircan et al. (1994) are close to those by Popper & Etzel.

In conclusion, the new photometric elements derived from analyses of the *uvby* light curves are significantly more accurate than previous determinations. We find that the secondary eclipse is almost total, with 98% of the y light of the secondary component eclipsed, whereas about 57% of the y light from the primary component is eclipsed at phase 0.0.

[4] http://www.astro.keele.ac.uk/∼jkt/

Table 5. Effective temperatures (K) for the combined light of BK Peg.

A_V	[Fe/H]	$(b-y)_0$	c_0	$(V-J)_0$	$(V-H)_0$	$(V-K_s)_0$	A96	H07	RM05	M06
0.188	−0.12	0.405	0.320	1.208	1.458	1.564	6280	6270	6270/6255/6130/6265	6290

NOTE 1: A_V is the adopted visual interstellar absorption. The V_0 magnitude and the $(b-y)_0$ and c_0 indices are based on the out-of-eclipse *uvby* standard indices from Table 1. The 2MASS observations (J, H, K_s) were obtained at phase 0.879.
NOTE 2: References are: A96 = Alonso et al. (1996). H07 = Holmberg et al. (2007). RM05 = Ramírez & Meléndez (2005). M06 = Masana et al. (2006).
NOTE 3: The results from A96 are based on their *uvby* calibration, those from RM05 on their *uvby*, $(V-J)$, $(V-H)$, and $(V-K_s)$ calibrations (in that order); the calibration by M06 is for $(V-K_s)$.

Table 6. Photometric solutions for BK Peg from the JKTEBOP code.

	y	b	v	u
i (°)	88.02 ±5	87.91 ±5	87.99 ±4	87.90 ±7
$e\cos\omega$	−0.00364 ±6	−0.00376 ±7	−0.00363 ±6	−0.00374 ±10
$e\sin\omega$	0.00283 ±181	0.00563 ±207	0.00438 ±183	0.00059 ±312
e	0.0046	0.0068	0.0057	0.0038
ω (°)	142.1	123.8	129.6	170.0
r_p	0.1092	0.1096	0.1092	0.1100
r_s	0.0806	0.0819	0.0807	0.0813
k	0.7379 ±50	0.7474 ±68	0.7394 ±46	0.7391 ±97
$r_p + r_s$	0.1898 ±5	0.1915 ±5	0.1900 ±4	0.1913 ±7
$u_p = u_s$	0.55	0.64	0.72	0.70
$y_p = y_s$	1.09	1.24	1.42	1.68
J_s/J_p	1.0444 ±31	1.0447 ±37	1.0569 ±34	1.1016 ±60
L_s/L_p	0.5670	0.5817	0.5756	0.5990
σ (mmag.)	4.8	5.2	4.7	7.9

NOTE 1: Linear limb darkening coefficients by Van Hamme (1993) were adopted, a mass ratio of 0.89 was assumed, and phase shift and mag. normalization were included as free parameters
NOTE 2: The errors quoted for the free parameters are the *formal* errors determined from the iterative least squares solution procedure

Table 7. Adopted photometric elements for BK Peg.

i	$87\overset{\circ}{.}96 \pm 0\overset{\circ}{.}14$
e	0.0053 ± 0.0013
ω	$138\overset{\circ}{.}7 \pm 19\overset{\circ}{.}0$
r_p	0.1094 ± 0.0004
r_s	0.0811 ± 0.0009
$r_p + r_s$	0.1906 ± 0.0012
k	0.741 ± 0.008

	y	b	v	u
J_s/J_p	1.044 ±4	1.048 ±4	1.057 ±4	1.095 ±6
L_s/L_p	0.572 ±11	0.574 ±14	0.578 ±10	0.599 ±15

NOTE: The individual flux and luminosity ratios are based on the mean stellar and orbital parameters

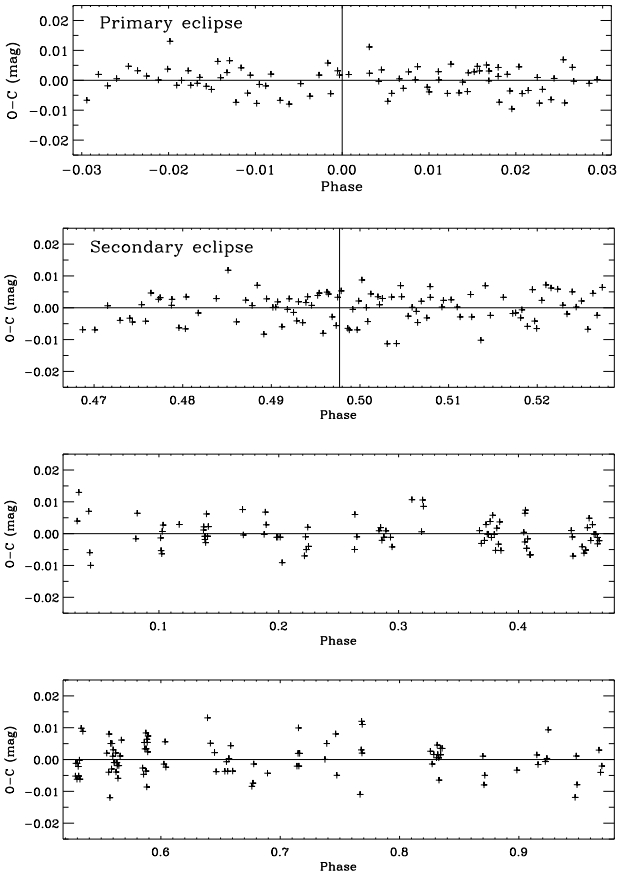

Fig. 2. $(O–C)$ residuals of the BK Peg y-band observations from the theoretical light curve computed for the photometric elements given in Table 6.

6. Spectroscopic elements

Spectroscopic orbits have been derived from a re-analysis of the radial velocities by Popper (1983) and an analysis of the new radial velocities listed in Table 4. We have used the method of Lehman-Filhés implemented in the SBOP[5] program (Etzel 2004), which is a modified and expanded version of an earlier code by Wolfe, Horak & Storer (1967). The orbital period P was fixed at the ephemeris value (Eq. 1), and the eccentricity e and longitude of periastron ω to the results from the photometric analysis (Table 7). The radial

[5] Spectroscopic Binary Orbit Program, `http://mintaka.sdsu.edu/faculty/etzel/`

Table 8. Spectroscopic orbital solutions for BK Peg.

Parameter:	Popper (re-analysis)	FIES (adopted)
Adjusted quantities:		
K_p (km s^{-1})	79.14 ± 0.33	78.77 ± 0.11
K_s (km s^{-1})	88.86 ± 0.56	88.59 ± 0.21
γ_p (km s^{-1})	-8.51 ± 0.30	-7.39 ± 0.08
γ_s (km s^{-1})	-8.35 ± 0.51	-7.20 ± 0.15
Adopted quantities:		
P (days)	5.48991046	5.48991046
T (HJD$-2\,400\,000$)[a]	50706.46968	50706.46968
e	0.0053	0.0053
ω (°)	138.7	138.7
Derived quantities:		
$M_p \sin^3 i$ ($M_\odot$)	1.427 ± 0.019	1.411 ± 0.007
$M_s \sin^3 i$ ($M_\odot$)	1.271 ± 0.013	1.255 ± 0.005
$q = M_s/M_p$	0.891 ± 0.007	0.889 ± 0.002
$a \sin i$ ($R_\odot$)	18.231 ± 0.071	18.161 ± 0.026
Other quantities pertaining to the fit:		
$N_{obs}(p/s)$	24/23	13/13
Time span (days)	1374	4
σ_p[b] (km s^{-1})	1.36	0.26
σ_s[b] (km s^{-1})	2.30	0.50

[a] Time of central primary eclipse
[b] Standard deviation of a single radial velocity

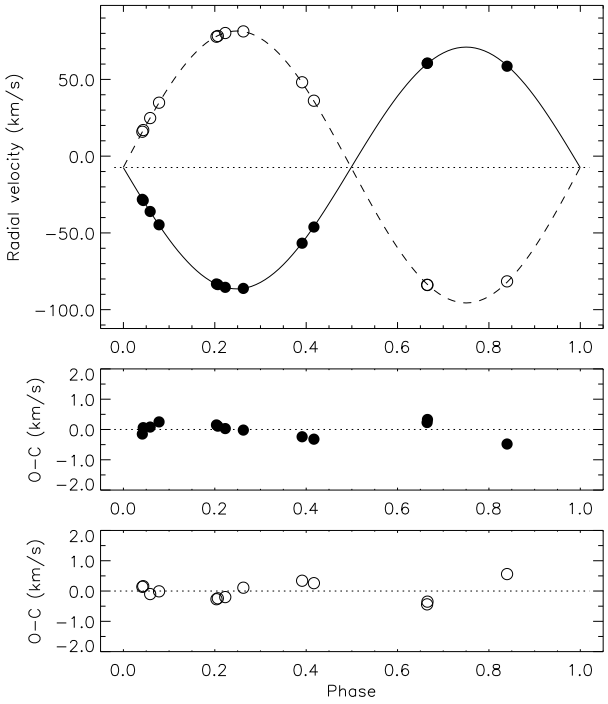

Fig. 3. Spectroscopic orbital solution for BK Peg (solid line: primary; dashed line: secondary) and radial velocities (filled circles: primary; open circles: secondary). The dotted line (upper panel) represents the center-of-mass velocity of the system. Phase 0.0 corresponds to central primary eclipse.

velocities of the components were analysed independently (SB1 solutions).

The spectroscopic elements are presented in Table 8. The semiamplitudes (K_p,K_s), and their uncertainties, obtained from Popper's velocities are identical to his results, even though he assumed the orbit to be circular and used an older ephemeris.

As seen, significantly more accurate semiamplitudes are derived from the FIES velocities. They are slightly smaller than those from Popper's velocities, but within errors the results agree. Including e and/or ω as free parameters formally improves the solution but does not alter the semiamplitudes. The number of velocities is, however, too small for reliable spectroscopic determination of e and ω. The double-lined (SB2) solutions agree perfectly with the single-lined solutions listed in Table 8. Also, spectroscopic elements determined as part of the spectral disentangling (Sect. 7) are identical. We notice that the new system velocities (γ_p,γ_s) differ by about 1 km s^{-1} from Popper's results. This is probably due to radial velocity zero point differences. Our velocities are tied to the ThAr exposures taken before and/or after each target exposure. Standard star observations normally agree to within 0.1–0.2 km s^{-1}.

7. Chemical abundances

For abundance analyses, we have disentangled the FIES spectra of BK Peg in order to extract the individual component spectra. We have applied the disentangling method introduced by Simon & Sturm (1994) and a revised version of the corresponding original code developed by E. Sturm. It assumes a constant light level, but since BK Peg is constant to within 0.5% outside of eclipses this is of no concern. Twenty-two orders, covering 5160–6450 Å (with a few gaps) were selected and disentangled individually. The orbital elements were fixed at the adopted values (Table 8) and very slightly wavelength dependent light ratios matching the results from the light curve analyses (Table 7) were adopted. Around 6070 Å, the signal-to-noise ratios of the resulting component spectra are 160 (primary) and 80 (secondary). A 40 Å region, centred at 6070 Å, is shown in Fig. 4

The basic approach followed in the abundance analyses is described by CTB08. We used the versatile VWA tool, which applies the SYNTH software (Valenti & Piskunov 1996) to compute synthetic spectra. We refer to Bruntt et al. (2004, 2008) and Bruntt (2009) for a detailed description of VWA. Atmosphere models were interpolated from the recent grid of MARCS model atmospheres (Gustafsson et al. 2008), which adopt the solar composition by Grevesse et al. (2007). Atomic line data are from the Vienna Atomic Line Database (VALD; Kupka et al. 1999), but in order to derive abundances relative to the Sun, $\log(gf)$ values have been adjusted in such a way that each measured line in the Wallace et al. (1998) Solar atlas reproduces the atmospheric abundances by Grevesse et al. (2007).

The abundance results derived from all useful lines with equivalent widths between 10 and 100 mÅ are presented in Table 9. The equivalent widths measured in the disentangled spectra are listed in Tables 14 (primary) and 15 (secondary), which will only be available in electronic form. The surface gravities and observed rotational veloci-

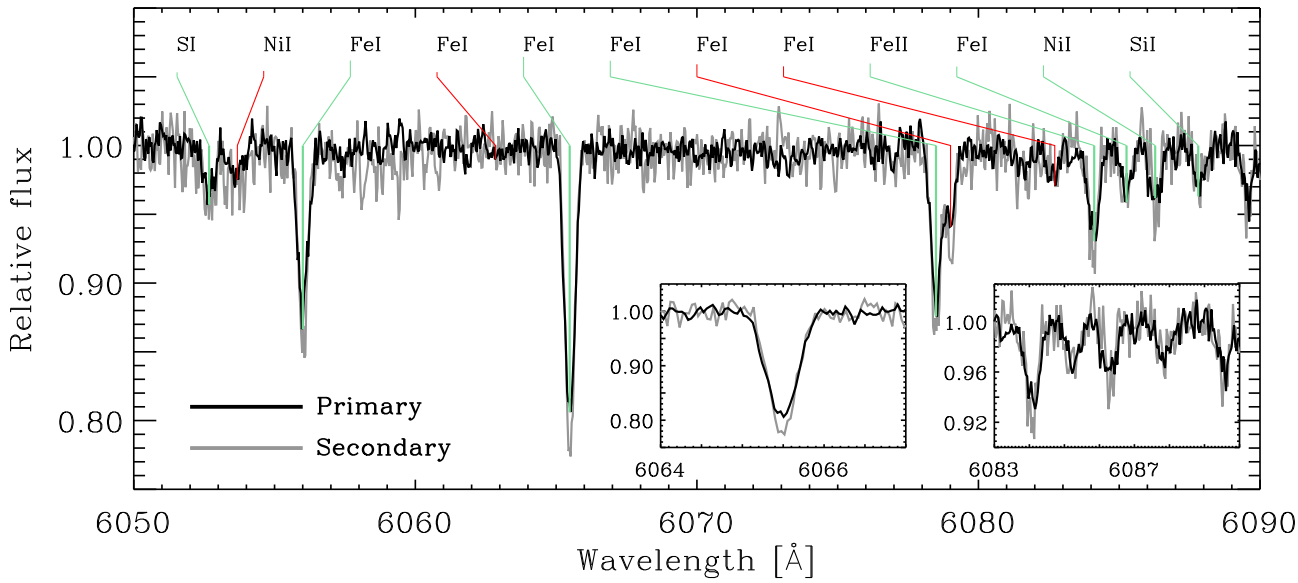

Fig. 4. A 40 Å region centred at 6070 Å of the disentangled spectra of the components of BK Peg. Lines identified by a red line were not used for the abundance analysis.

Table 9. Abundances ([El./H]) for the primary and secondary components of BK Peg.

	Primary			Secondary		
Ion	[El./H]	rms	N[a]	[El./H]	rms	N[a]
Si I	−0.19	0.05	12	−0.12	0.09	10
Ca I	−0.05	0.05	4	0.00	0.07	6
Sc II	−0.14	0.09	3	−0.18	0.09	3
Ti I				−0.17	0.06	3
Ti II	−0.07	0.09	3	0.01	0.18	3
Cr I	−0.20	0.03	3	−0.19	0.03	3
Cr II	−0.23	0.05	3	−0.04	0.03	4
Fe I	−0.12	0.07	78	−0.12	0.09	70
Fe II	−0.15	0.09	10	−0.11	0.11	12
Ni I	−0.23	0.08	6	−0.24	0.13	11

[a] Number of lines used per ion

ties listed in Table 10 were adopted, whereas the effective temperatures and microturbulence velocities were tuned until Fe I abundances were independent of line equivalent widths and excitation potentials. The resulting temperatures are 6365 ± 50 K (primary) and 6385 ± 50 K (secondary). From a study of 10 F-K type stars with interferometrically and spectroscopically determined effective temperatures, Bruntt et al. (2010) find a systematic offset of 40 K, which should be subtracted. The corrected spectroscopic temperatures are still slightly higher than derived from the *uvby* indices (Table 10) but agree within errors.

Microturbulence velocities of 1.55 ± 0.25 km s^{-1} (primary) and 1.22 ± 0.25 km s^{-1} (secondary) were obtained. The calibration by Edvardsson et al. (1993) predicts higher values of 2.20±0.31 km s^{-1} (primary) and 1.95±0.31 km s^{-1} (secondary); the difference in microturbulence will be discussed by Bruntt et al. (2010).

As seen, a robust [Fe/H] is obtained, with nearly identical results from Fe I and Fe II lines of both components. The mean value from all measured Fe lines is [Fe/H] = −0.12 ± 0.01 (rms of mean). Changing the model temperatures by ±50 K modifies [Fe/H] from the Fe I lines by about ±0.05 dex, whereas almost no effect is seen for Fe II lines. If 0.25 km s^{-1} higher microturbulence velocities are adopted, [Fe/H] decreases by about 0.04 dex for both neutral and ionized lines. Taking these contributions to the uncertainties into account, we adopt [Fe/H] = −0.12 ± 0.07 for BK Peg. In general, we find similar relative abundances for the other ions listed in Table 9, including the α-elements Si, Ca, and Ti.

As an addition to the spectroscopic abundance analysis, we have also calculated metal abundances from the de-reddened *uvby* indices for the individual components (Table 10) and the calibration by Holmberg et al. (2007). The results are: [Fe/H] = −0.07 ± 0.18 (primary) and [Fe/H] = −0.14 ± 0.20 (secondary). Within errors they agree with those from the spectroscopic analysis; the quoted [Fe/H] errors include the uncertainties of the photometric indices and the published spread of the calibration.

8. Absolute dimensions

Absolute dimensions for BK Peg are presented in Table 10, as calculated from the photometric and spectroscopic elements given in Tables 7 and 8. As seen, masses and radii precise to 0.4–0.5% and 0.4–1.2%, respectively, have been established for the binary components.

The V magnitudes and *uvby* indices for the components, included in Table 10, were calculated from the combined magnitude and indices of the system outside eclipses (Table 1) and the luminosity ratios between the components (Table 7). Within errors, the V magnitude and the *uvby* indices of the primary component agree with those measured at central secondary eclipse where 98% (y) of the light from the secondary component eclipsed (cf. Table 1).

Table 10. Astrophysical data for BK Peg.

	Primary	Secondary
Absolute dimensions:		
$M/M_\odot$	1.414 ± 0.007	1.257 ± 0.005
$R/R_\odot$	1.988 ± 0.008	1.474 ± 0.017
$\log g$ (cgs)	3.992 ± 0.004	4.201 ± 0.010
$v \sin i$[a] ($\mathrm{km\,s^{-1}}$)	16.6 ± 0.2	13.4 ± 0.2
v_{sync}[b] ($\mathrm{km\,s^{-1}}$)	18.3 ± 0.1	13.6 ± 0.2
v_{psync}[c] ($\mathrm{km\,s^{-1}}$)	18.3 ± 0.1	13.6 ± 0.2
v_{peri}[d] ($\mathrm{km\,s^{-1}}$)	18.5 ± 0.1	13.7 ± 0.2
Photometric data:		
V[e]	10.473 ± 0.009	11.080 ± 0.014
$(b-y)$[e]	0.363 ± 0.007	0.360 ± 0.008
m_1[e]	0.144 ± 0.013	0.139 ± 0.016
c_1[e]	0.466 ± 0.014	0.436 ± 0.017
$E(b-y)$	0.044 ± 0.015	
$T_{\rm eff}$	6265 ± 85	6320 ± 90
$M_{\rm bol}$	2.90 ± 0.06	3.51 ± 0.07
$\log L/L_\odot$	0.74 ± 0.02	0.49 ± 0.03
$B.C.$	-0.01	-0.01
M_V	2.91 ± 0.06	3.52 ± 0.07
$V_0 - M_V$	7.37 ± 0.09	7.37 ± 0.10
Distance (pc)	298 ± 12	298 ± 13
Abundance:		
[Fe/H]	-0.12 ± 0.07	

[a] Observed rotational velocity
[b] Equatorial velocity for synchronous rotation
[c] Equatorial velocity for pseudo-synchronous rotation
[d] Refers to periastron velocity
[e] Not corrected for interstellar absorption/reddening

NOTE: Bolometric corrections (BC) by Flower (1996) have been assumed, together with $T_{eff\odot} = 5780$ K, $BC_\odot = -0.08$, and $M_{bol\odot} = 4.74$.

Table 11. Model parameters and average ages for BK Peg inferred from the observed masses and radii.

Grid	[Fe/H]	Y	Z	Age (Gyr)
Yonsei-Yale	-0.190	0.2540	0.0120	2.55
	-0.120	0.2580	0.0140	2.70
	-0.105	0.2590	0.0145	2.75
	-0.050	0.2626	0.0163	2.85
Victoria-Regina	-0.190	0.2629	0.0125	2.35
	-0.105	0.2684	0.0150	2.50
	-0.039	0.2735	0.0173	2.60

The interstellar reddening $E(b-y) = 0.044 \pm 0.015$, also given in Table 10, was determined from the calibration by Olsen (1988), using the $uvby\beta$ standard photometry for the combined light outside eclipses. Within errors, the same reddening is obtained from the indices observed during the central part of secondary eclipse. The new intrinsic-colour calibration by Karatas & Schuster (2009) leads to $E(b-y) = 0.034$. The model by Hakkila et al. (1997) yields a higher reddening of $E(B-V) = 0.14$ or $E(b-y) = 0.10$ in the direction of and at the distance of BK Peg, whereas the maps by Burstein & Heiles (1982) and Schlegel et al. (1998) give *total* $E(B-V)$ reddenings of 0.07 and 0.05, respectively.

From the individual indices and the calibration by Holmberg et al. (2007), we derive effective temperatures of 6265 ± 85 and 6285 ± 90 K for the primary and secondary component, respectively, assuming the final [Fe/H] abundance. The temperature uncertainties include those of the $uvby$ indices, $E(b-y)$, [Fe/H], and the calibration itself. Compared to this, the empirical flux scale by Popper (1980) and the y flux ratio between the components (Table 7) yield a well established temperature difference between the components of 55 ± 5 K (excluding possible errors of the scale itself). Consequently, we assign temperatures of 6265 and 6320 K, which agree with the corrected spectroscopic results, 6325 and 6345 K, within errors (Sect.7). As seen from Table 5 (combined light), temperatures from the $(b-y)$, c_1 calibration by Alonso et al. (1996) and the $b-y$ calibration by Ramírez & Meléndez (2005) are in perfect agreement with that from the Holmberg et al. calibration.

The measured rotational velocity for the secondary component is in perfect agreement with (pseudo)synchronous rotation, whereas the primary component seems to rotate at a slightly lower rate.

The distance to BK Peg was calculated from the "classical" relation (see e.g. CTB08), adopting the solar values and bolometric corrections given in Table 10, and $A_V/E(b-y) = 4.28$ (Crawford & Mandwewala 1976). As seen, identical values are obtained for the two components, and the distance has been established to 4%, accounting for all error sources. Nearly the same distance is obtained if other BC scales, e.g. Code et al. (1976), Bessell et al. (1998) and Girardi et al. (2002), are adopted. Also, the empirical K surface brightness - $T_{\rm eff}$ relation by Kervella et al. (2004) leads to an identical and perhaps even more precise (2%) distance. We refer to Clausen (2004) and Southworth et al. (2005) for details on the use of eclipsing binaries as standard candles.

9. Comparison with stellar models

In the following, we compare the absolute dimensions obtained for BK Peg with properties of recent theoretical stellar evolutionary models. We have concentrated on the Yonsei-Yale (Y^2) grids by Demarque et al. (2004)[6] and the VRSS (scaled-solar abundances of the heavy elements) Victoria-Regina grids (VandenBerg et al., 2006)[7] listed in Table 11. The abundance, mass, and age interpolation routines provided by the Y^2 group and the isochrone interpolation routines provided by the Victoria-Regina group have been applied. A summary of the Y^2 and VRSS grids and their input physics is given by CTB08. Here we just recall the following: The Y^2 models include He diffusion, whereas diffusion processes are not included in the VRSS models. The Y^2 models adopt the enrichment law $Y = 0.23 + 2Z$ together with the solar mixture by Grevesse et al. (1996), and the VRSS models $Y = 0.23544 + 2.2Z$ and the solar mixture by Grevesse & Noels (1993).

Both grids include core overshoot. For the Y^2 models, $\Lambda_{OS} = \lambda_{\rm ov}/H_{\rm p}$ depends on mass and also takes into ac-

[6] `http://www.astro.yale.edu/demarque/yystar.html`
[7] `http://www1.cadc-ccda.hia-iha.nrc-cnrc.gc.ca/cvo/community/VictoriaReginaModels/`

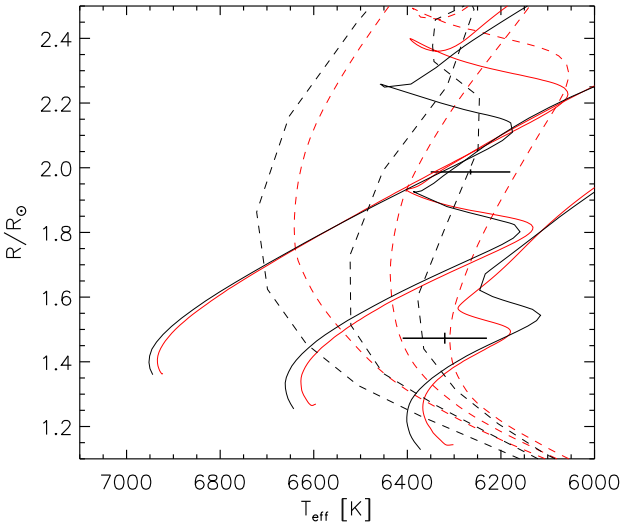

Fig. 5. Comparison between Y^2 (black) and VRSS (red) models for [Fe/H] = −0.105. Tracks (solid lines) for 1.2, 1.3, and 1.4 $M_\odot$ and isochrones (dashed lines) for 2.0, 2.5, and 3.0 Gyr are included. The 1.26 and 1.41 $M_\odot$ components of BK Peg are shown.

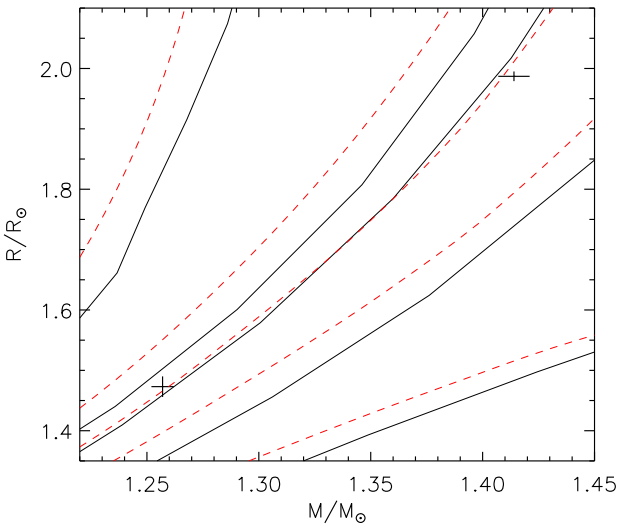

Fig. 6. Comparison between Y^2 (solid lines, black) and VRSS (dashed lines, red) models for [Fe/H] = −0.105. Isochrones for 1.0, 2.0, 2.5 (VRSS only), 2.75 (Y^2 only), 3.0, and 4.0 Gyr are included. The 1.26 and 1.41 $M_\odot$ components of BK Peg are shown.

count the composition dependence of $M_{\rm crit}^{\rm conv}$ [8]. The ramping of $\Lambda_{OS} = \lambda_{\rm ov}/H_{\rm p}$ from 0 at $M_{\rm crit}^{\rm conv}$ to 0.2 at $1.2 \times M_{\rm crit}^{\rm conv}$ and higher masses is done in steps of 0.05. For the metallicity of BK Peg, $M_{\rm crit}^{\rm conv}$ is 1.2 $M_\odot$. The Victoria-Regina group adopts a somewhat different physically based description of the core overshoot with the free parameter $F_{\rm over}$ depending on mass and metallicity and calibrated observationally via

[8] Defined as "the mass above which stars continue to have a substantial convective core even after the end of the pre-MS phase."

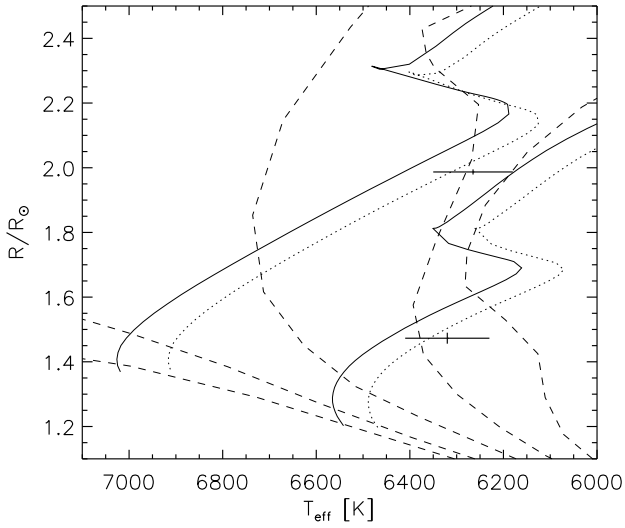

Fig. 7. BK Peg compared with Y^2 models for [Fe/H] = −0.12. Tracks for the component masses (solid lines) and isochrones for 0.5 and 1.0–4.0 Gyr (dashed; step 1.0 Gyr) are shown. Tracks (dotted) for [Fe/H] = −0.05 are included.

cluster CMDs. For the metallicity of BK Peg, core convection sets in around 1.15 $M_\odot$, and $F_{\rm over}$ gradually increases to 0.55 at 1.70 $M_\odot$ and is kept at this value for higher masses. Thus, for both grids, the 1.26 and 1.41 $M_\odot$ components of BK Peg are in their ramping regions.

In Fig. 5, we compare Y^2 and VRSS main-sequence evolutionary tracks and isochrones for [Fe/H] = −0.105[9] in the mass region of BK Peg. For 1.3 $M_\odot$ the tracks nearly coincide, whereas the TAMS positions differ for both lower and higher masses, probably related to the individual core overshoot recipes. In addition, somewhat different ages are predicted along the main-sequence tracks. This is also illustrated by the isochrones in the mass-radius diagram shown in Fig. 6, which represents the most direct comparison with BK Peg, since the observed masses and radii are scale independent. As seen, similar ages of 2.75 (Y^2) and 2.50 (VRSS) Gyr are predicted for the components, with a slight preference for the shape of the VRSS isochrone. Within the observed metal abundance range, [Fe/H] = −0.12 ± 0.07, the best fitting isochrones reproduce BK Peg nearly equally well; the corresponding average ages are listed in Table 11.

Y^2 tracks for the observed masses and abundance of BK Peg are shown in Fig. 7. They are, like the VRSS tracks, slightly hotter. We also recall that the temperatures derived as part of the spectroscopic abundance analysis are slightly higher than those adopted from the *uvby* indices (Table 10).

In conclusion, the Y^2 and Victoria-Regina VRSS models, including their core overshoot treatment and ramping recipes, are able to reproduce the observed properties of BK Peg. We note, however, that both grids predict a slightly lower age for the 1.41 $M_\odot$ primary component than for the 1.26 $M_\odot$ secondary. In the following section, we will check whether this tendency is seen for other well-studied binaries with similar component masses.

[9] VRSS models for the observed [Fe/H] = −0.12 are not available

Table 12. Masses, radii, and abundances from Torres et al. (2009) for a subset of well-studied binaries with both components in the 1.15–1.70 $M_\odot$ interval; see the text for details.

System	Colour Figs. 9, 10	M_{pri} ($M_\odot$)	R_{pri} ($R_\odot$)	M_{sec} ($M_\odot$)	R_{sec} ($R_\odot$)	[Fe/H] observed	[Fe/H] Y^2	Age (Gyr) Y^2	[Fe/H] VRSS	Age (Gyr) VRSS
GX Gem	cyan	1.488 ±11	2.326 ±12	1.467 ±10	2.236 ±12		0.00	2.79	0.000	2.55
BK Peg	black	1.414 ±7	1.987 ±8	1.257 ±5	1.473 ±17	−0.12 ±7	−0.12	2.70	−0.105	2.50
BW Aqr	magenta	1.377 ±21	1.786 ±43	1.479 ±19	2.062 ±44	−0.07 ±11	−0.08	2.43	−0.105	2.15
V442 Cyg	red	1.560 ±24	2.073 ±34	1.407 ±23	1.663 ±33		−0.10	1.77	−0.105	1.65
AD Boo	green	1.414 ±9	1.612 ±14	1.209 ±6	1.216 ±10	+0.10 ±15	+0.10	1.77	+0.136	1.50
FS Mon	orange	1.632 ±10	2.052 ±12	1.462 ±10	1.629 ±10		+0.23	1.44	+0.226	1.23
VZ Hya	brown	1.271 ±9	1.314 ±5	1.146 ±6	1.113 ±7	−0.20 ±12	−0.20	1.20	−0.190	0.90
V570 Per	blue	1.447 ±9	1.521 ±34	1.347 ±8	1.386 ±19	+0.02 ±3	+0.02	1.00	0.000	0.75
HD71636	gray	1.514 ±7	1.571 ±26	1.288 ±6	1.363 ±26		0.00	0.80/1.70	0.000	0.70/1.30

10. Comparison with other binaries

The review on accurate masses and radii of normal stars by Torres et al. (2009) lists 20 binaries[10] with both components in the 1.15–1.70 $M_\odot$ interval where core overshoot is ramped up in the Y^2 and Victoria-Regina models. Here, we will concentrate on the subset listed in Table 12, where most of the nearly equal-mass binaries have been excluded. Eight binaries have been selected because the masses of their components differ significantly; we have adopted a lower mass difference limit of 0.10 $M_\odot$. In addition, we have included GX Gem, since its components have evolved close to the TAMS region. As mentioned in Sect. 1, Lacy et al. (2008) found that for GX Gem, the lowest $\alpha_{\rm ov}$ consistent with observations is approximately 0.18. [Fe/H] has been measured for five of the systems; we refer to Appendix A for details on the abundance analysis of BW Aqr.

Fig. 8 shows the nine binaries together with Y^2 evolutionary tracks for the measured masses. For GX Gem, V442 Cyg, FS Mon, and HD 71636, [Fe/H] has not been measured. The values listed in Table 12 were adopted only because they lead to reasonable model fits for the observed effective temperatures. The isochrones correspond to the average age inferred from the measured masses and radii. To illustrate the abundance dependence, evolutionary tracks and isochrones for solar metallicity have been included for V442 Cyg and FS Mon. As seen, the nine binaries cover the main-sequence almost from the ZAMS to the TAMS.

In Figs. 9 (Y^2) and 10 (VRSS), we concentrate on comparisons based on the scale-independent masses and radii. Since abundance interpolation software is not available for the VRSS models, we have used those with [Fe/H] closest to the measured values. The average ages are listed in Table 12, and we note the following:

- The VRSS models predict lower ages than the Y^2 models for all systems.
- For the four binaries with components in the upper half of the main-sequence band (GX Gem, BK Peg, BW Aqr, V442 Cyg), both grids tend to predict lower ages for the more massive component than for the less massive one, although the difference is certainly very marginal for the nearly equal-mass system GX Gem. These systems span the 1.26–1.56 $M_\odot$ interval.
- The Y^2 isochrones fit FS Mon (1.63 + 1.46 $M_\odot$) better than the VRSS isochrones, which predict a higher age for the more massive component than for the less massive one.
- Both grids fit the less evolved binaries AD Boo and VZ Hya quite well, perhaps with a slight preference for Y^2.
- For the little evolved binary V570 Per, VRSS is marginally better than Y^2.
- HD 71636 is not fitted well by any of the grids. The very different ages predicted for the components are listed in Table 12. We believe, however, that this is due to problems with the published radii. A re-analysis of the light curves by Henry et al. (2006) indicates that the ratio between the (relative) radii is significantly more uncertain than given by the authors[11], most probably because the secondary eclipse is far from being well-covered.

It is outside the scope of this paper to propose specific modifications of the model physics, but we believe that this sample of binaries (except HD 71636) can be used to fine-tune the core overshoot treatment in terms of mass and metal abundance. It might also be relevant to include investigations of other model ingredients, e.g. diffusion processes and the adopted helium-to-metal enrichment ratio, and to clarify why the Y^2 models predict higher ages than the VRSS models. In order to avoid possible interpolation errors, specific models for the observed masses and metal abundances should be calculated and small age steps applied. On the observational side, spectroscopic metal abun-

[10] The 20 binaries can now be supplemented by BK Peg and V1130 Tau (Clausen et al. 2010).

[11] We have used the larger errors listed by Torres et al. (2009), which also seem to be underestimated.

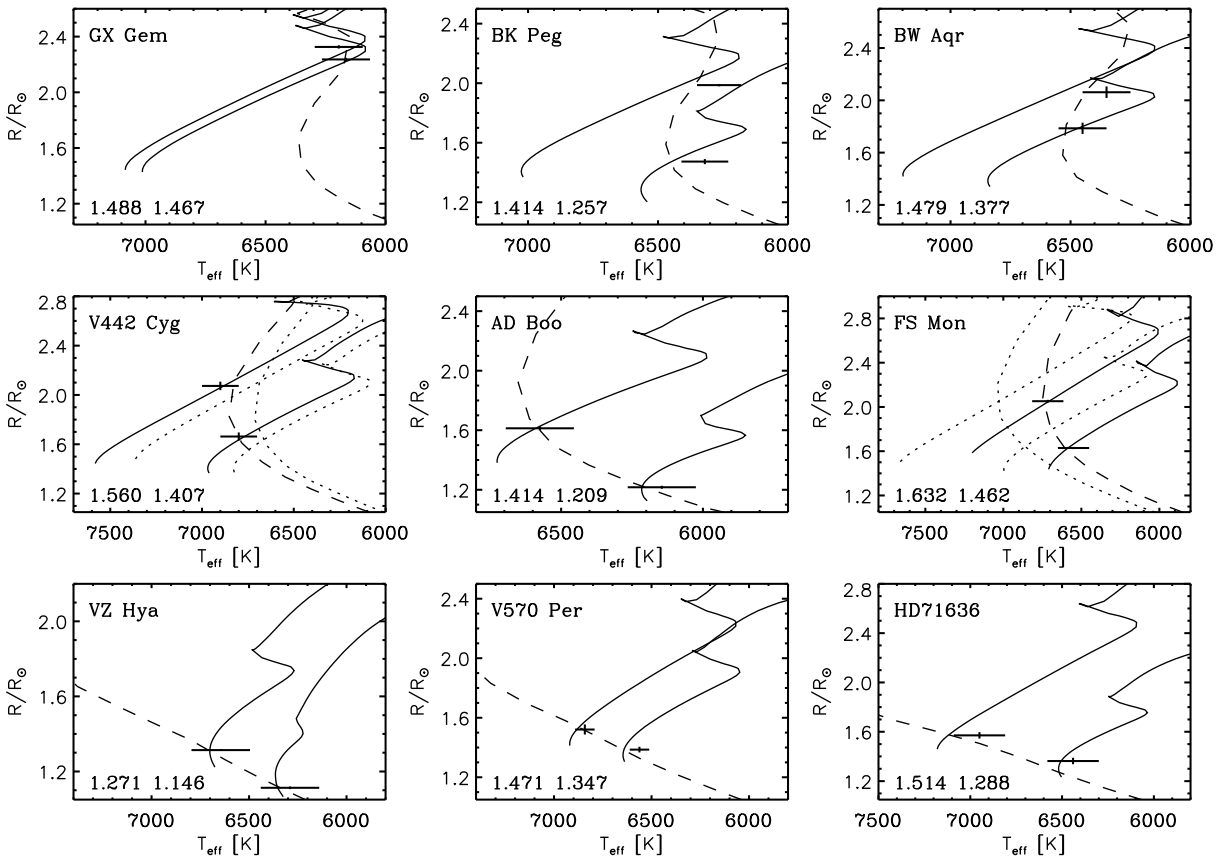

Fig. 8. Y^2 evolutionary tracks (full drawn lines) for the binaries included in Table 12. The isochrones (dashed lines) correspond to the average ages inferred from the masses and radii for the [Fe/H] listed in the table. For HD 71636, the 0.80 Gyr isochrone is plotted. For V442 Cyg and FS Mon, the dotted tracks and isochrones (1.83 and 1.38 Gyr, respectively) represent solar abundance models. Component masses (in units of $M_{\odot}$) are given in the lower left corners.

dances should be determined for the four binaries lacking this information, and it should perhaps be considered to re-observe BW Aqr, V442 Cyg, and HD 71636 to improve their masses and/or radii.

Also, we suggest to supplement the sample by the unique K0IV+F7V binary AI Phe ($1.23 + 1.19\ M_{\odot}$), recently re-discussed by Torres et al. (2009), as well as by a number of new F-type systems we are presently studying. In addition, it would be highly relevant to include F-type binary members of open clusters.

11. Summary and conclusions

From state-of-the-art observations and analyses, precise (0.4–1.2%) absolute dimensions have been established for the components of the late F-type detached eclipsing binary BK Peg ($P = 5\overset{\mathrm{d}}{.}49$, $e = 0.0053$); see Table 10. A detailed spectroscopic analysis yields an iron abundance relative to the Sun of $[\mathrm{Fe/H}] = -0.12 \pm 0.07$ and similar relative abundances for Si, Ca, Sc, Ti, Cr, and Ni. The measured rotational velocities are 16.6 ± 0.2 (primary) and 13.4 ± 0.2 (secondary) km s^{-1}. For the secondary component this corresponds to (pseudo)synchronous rotation, whereas the primary component seems to rotate at a slightly lower rate.

The 1.41 and 1.26 $M_{\odot}$ components of BK Peg have evolved to the upper half of the main-sequence band. Yonsei-Yale and Victoria-Regina solar scaled evolutionary models for the observed metal abundance reproduce BK Peg at ages of 2.75 and 2.50 Gyr, respectively, but tend to predict a lower age for the more massive primary component than for the secondary. If real, this might be due to less than perfect calibration of the amount of convective core overshoot of the models as function of mass (and metal abundance).

For this reason, we have performed model comparisons for a sample of eight additional well-studied binaries with component masses in the 1.15–1.70 $M_{\odot}$ interval where convective core overshoot is gradually ramped up in the models; see Table 12. We find that *a*) the Yonsei-Yale models systematically predict higher ages than the Victoria-Regina models, and that *b*) the three other most evolved systems in the sample share the age difference trend seen for BK Peg.

We propose to use the sample to fine-tune the core overshoot treatment, as well as other model ingredients, and to clarify why the two model grids predict different ages. The sample should be expanded by a number of new F-type systems under study, binary cluster members, and the unique K0IV+F7V binary AI Phe ($1.23+1.19\ M_{\odot}$).

Acknowledgements. It is a great pleasure to thank the many colleagues and students, who have shown interest in our project and have participated in the extensive (semi)automatic observations of BK Peg at the SAT: Sylvain Bouley, Christian Coutures, Thomas H. Dall, Mathias P. Egholm, Pascal Fouque, Lisbeth F. Grove, Anders Johansen, Erling Johnsen, Bjarne R. Jørgensen, Bo Milvang-Jensen, Alain Maury, John D. Pritchard, and Samuel Regandell. Excellent technical support was received from the staffs of Copenhagen

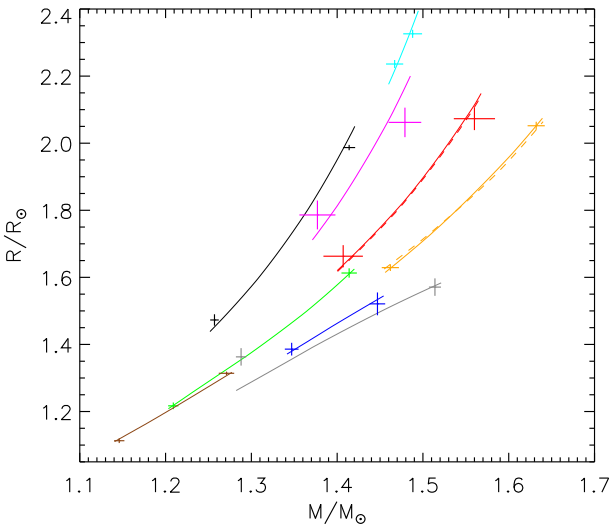

Fig. 9. Comparison between Y^2 isochrones (full drawn lines) and the binaries listed in Table 12; we refer to the table for colour codes, [Fe/H] and ages. For V442 Cyg and FS Mon, the dashed lines are solar abundance isochrones for 1.83 and 1.38 Gyr, respectively. For HD 71636, the 0.80 Gyr isochrone is plotted.

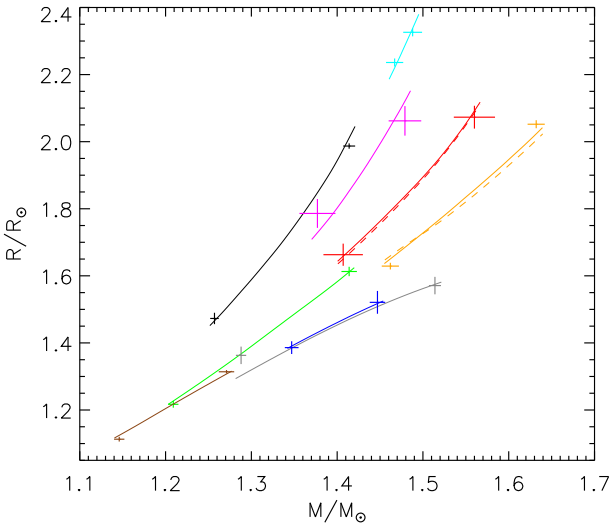

Fig. 10. Comparison between VRSS isochrones (full drawn lines) and the binaries listed in Table 12; we refer to the table for colour codes, [Fe/H] and ages. For V442 Cyg and FS Mon, the dashed lines are solar abundance isochrones for 1.67 and 1.27 Gyr, respectively. For HD 71636, the 0.70 Gyr isochrone is plotted.

University and ESO, La Silla. We thank J. M. Kreiner for providing a complete list of published times of eclipse for BK Peg. A. Kaufer, O. Stahl, S. Tubbesing, and B. Wolf kindly obtained the two FEROS spectra of BW Aqr during Heidelberg/Copenhagen guaranteed time in 1999.

The projects "Stellar structure and evolution – new challenges from ground and space observations" and "Stars: Central engines of the evolution of the Universe", carried out at Copenhagen University and Aarhus University, are supported by the Danish National Science Research Council.

The following internet-based resources were used in research for this paper: the NASA Astrophysics Data System; the SIMBAD database and the VizieR service operated by CDS, Strasbourg, France; the arχiv scientific paper preprint service operated by Cornell University; the VALD database made available through the Institute of Astronomy, Vienna, Austria; the MARCS stellar model atmosphere library. This publication makes use of data products from the Two Micron All Sky Survey, which is a joint project of the University of Massachusetts and the Infrared Processing and Analysis Center/California Institute of Technology, funded by the National Aeronautics and Space Administration and the National Science Foundation.

References

Ak, H., Ozerer, F. F., & Ekmekci, F. 2003, Inf. Bull. Var. Stars, 5361
Alonso, A., Arribas, S., & Martínez-Roger, C. 1996, A&A, 313, 873
Andersen, J., Nordström, B., & Clausen, J. V. 1990, ApJ, 363, L33
Bessell, M. S., Castelli, F., & Plez, B. 1998, A&A, 333, 231
Braune, W., & Hübscher, J. 1987, BAV Mitteilungen, 46
Bruntt, H. 2009, A&A, 506, 235
Bruntt, H., Bikmaev, I. F., Catala, C., et al. 2004, A&A, 425, 683
Bruntt, H., De Cat, P., & Aerts, C. 2008, A&A, 478, 487
Bruntt, H., Bedding, T. R., Quirion, P.-O., et al. 2010, astro-ph/10024268
Burstein, D., & Heiles, C. 1982, AJ, 87, 1165
Claret, A. 2000, A&A, 363, 1081
Claret, A. 2007, A&A, 475, 1019
Clausen, J. V. 1991, A&A, 246, 397
Clausen, J. V. 2004, New A Rev., 48, 679
Clausen, J. V., Helt, B. E., & Olsen, E. H. 2001, A&A, 374, 980 (CHO01)
Clausen, J. V., Torres, G., Bruntt, H., et al. 2008b, A&A, 487, 1095 (CTB08)
Clausen, J. V., Olsen, E. H., Helt, B. E., & Claret, A. 2010, A&A, in press
Code, A. D., Bless, R. C., Davis, J., & Brown, R. H. 1976, ApJ, 203, 417
Crawford, D. L., & Mandwewala, N. 1976, PASP, 88, 917
Demarque, P., Woo, J.-H., Kim, Y.-C., & Yi, S. K. 2004, ApJS, 155, 667
Demircan, O., Kaya, Y., & Tüfekcioglu, Z. 1994, Ap&SS, 222, 213
Diethelm, R. 2001, in BBSAG Bulletin, 126
Dworak, T. Z. 1977, Acta Astron., 27, 151
Edvardsson, B., Andersen, J., Gustafsson, B., et al. 1993, A&A, 275, 101
Etzel P. B. 1981, in Photometric and Spectroscopic Binary Systems, ed. E.B. Carling, & Z. Kopal, (NATO), 111
Etzel, P. B. 2004, SBOP: Spectroscopic Binary Orbit Program (San Diego State University)
Flower, P. J. 1996, ApJ, 469, 355
Girardi, L., Bertelli, G., Bressan, A., et al. 2002, A&A, 391, 195
Grevesse, N., & Noels, A. 1993, Phys. Scr. T47, 133
Grevesse, N., & Sauval, A. J. 1998, Space Sci. Rev., 85, 161
Grevesse, N., Noels, A., & Sauval, A. J. 1996, in Cosmic Abundances, ed. S.S. Holt, & G. Sonneborn (San Francisco: ASP), 117
Grevesse, N., Asplund, M., & Sauval, A. J. 2007, Space Sci. Rev., 130, 105
Griffin, R. F. 2007, The Observatory, 127, 113
Gustafsson, B., Edvardsson, B., Eriksson, K., et al. 2008, A&A, 486, 951
Hakkila, J., Myers, J. M., Stidham, B. J., & Hartmann, D. H. 1997, AJ, 114, 2043
Harlan, E. A. 1969, AJ, 74, 916
Harlan, E. A., & Taylor, D. C. 1970, AJ, 75, 507
Heard, J. F. 1956, Publ. David Dunlop Obs., 2, 105
Heiter, U., Kupka, F., van't Menneret, C., et al. 2002, A&A, 392, 619
Henry, G. W., Fekel, F. C., Sowell, J. R., & Gearhart, J. S. 2006, AJ, 132, 2489
Hoffmeister, C. 1931, AN 242, 129
Holmberg, J., Nordström, B., & Andersen, J. 2007 A&A, 475, 519
Hübscher, J., & Walter, F. 2007, Inf. Bull. Var. Stars, 5761
Jordi, C., Figueras, F., Torra, J., & Asiain, R. 1996, A&AS, 115, 401
Kaluzny, J., Pych, W., Rucinski, S. M., & Thompson, I. B. 2006, Acta Astron., 56, 237
Karatas, Y., & Schuster, W. J. 2010, New A, 15, 444

Kervella, P., Thévenin, F., Di Folco, E., & Ségransan, D. 2004, A&A, 426, 297
Kreiner, J. M. 2004, Acta Astron., 54, 207
Kreiner, J. M., Kim, C. H., & Nha, I. S. 2001, An Atlas of O−C Diagrams of Eclipsing Binary Stars (Krakow: Wydawnictwo Naukowe Akad. Pedagogicznej)
Kupka, F., Piskunov, N., Ryabchikova, T. A., Stempels, H. C., & Weiss, W. 1999, A&AS, 138, 119
Lacy, C. H. S., Torres, G., & Claret, A. 2008, AJ, 135, 1757
Lause, F. 1935, AN 257, 73
Lause, F. 1937, AN 263, 115
Martynov D. Ya. 1973, in Eclipsing Variable Stars, ed. V. P. Tsesevich, Israel Program for Scientific Translation, Jerusalem
Masana, E., Jordi, C., & Ribas, I. 2006, A&A, 450, 735
Nelson B., & Davis W. 1972, ApJ, 174, 617
Olsen, E. H. 1983, A&AS, 54, 55
Olsen, E. H. 1988, A&A, 189, 173
Olsen, E. H. 1994, A&AS, 106, 257
Perry, C. L. 1969, AJ, 74, 705
Popper, D. M. 1980, ARA&A 18, 115
Popper, D. M. 1983, AJ, 88, 124
Popper, D. M., & Dumont, P. J. 1977, AJ, 82, 216
Popper, D. M., & Etzel, P. B. 1981, AJ, 86, 102
Popper, D. M., & Etzel, P. B. 1995, Ap&SS, 232, 139
Ramírez, I., & Meléndez, J. 2005, AJ, 626, 465
Ribas, I., Jordi, C., & Giménez, A. 2000, MNRAS, 318, 55
Rucinski, S. M. 1999, in Precise Stellar Radial Velocities, ed. J. B. Hearnshaw, & C. D. Scarfe, IAU Coll. 170, ASP Conf. Ser., 185, 82
Rucinski, S. M. 2002, AJ, 124, 1746
Rucinski, S. M. 2004, in Stellar Rotation, ed. A. Maeder, & P. Eenens, IAU Symp. 215, (San Francisco: ASP), 17
Schlegel, D. J., Finkbeiner, D. P., & Davis, M. 1998, ApJ, 500, 525
Simon, K. P., & Sturm, E. 1994, A&A, 1994, 281
Southworth, J., Maxted, P. F. L., & Smalley, B. 2004a, MNRAS, 351, 1277
Southworth, J., Zucker, S., Maxted, P. F. L., & Smalley, B. 2004b, MNRAS, 355, 986
Southworth, J., Maxted, P. F. L., & Smalley, B. 2005, A&A, 429, 645
Torres, G., Andersen, J., & Giménez, A. 2009, A&A Rev., in press
Valenti, J., & Piskunov, N. 1996, A&AS, 118, 595
VandenBerg, D. A., Bergbusch, P. A., & Dowler, P. D. 2006, ApJS, 162, 375
Van Hamme, W. 1993, AJ, 106, 2096
Wallace, L., Hinkle, K., & Livingston, W. 1998, An atlas of the spectrum of the solar photosphere from 13500 to 28000 cm $^{-1}$ (3570 to 7405 A), Tucson, AZ: NOAO
Wolfe, R. H., Horak, H. G., & Storer, N. W. 1967, in Modern Astrophysics: A Memorial to Otto Struve, ed. M. Hack, 251

Appendix A: Chemical abundances for BW Aqr

Absolute dimensions for the late F-type eclipsing binary BW Aqr were published by Clausen (1991), who mentioned that the *uvbyβ* photometry indicates a metallicity slightly above solar. We note that the primary component (star A in Clausen 1991), eclipsed at the deeper minimum at phase 0.0, is less massive, smaller, but hotter than the secondary component.

Here we present the results from an abundance analysis based on two high-resolution spectra observed with the FEROS fibre echelle spectrograph at ESO, La Silla in August 1999; see Table A.1. Details on the spectrograph, the reduction of the spectra, and the basic approach followed in the abundance analysis are described by CTB08. As for BK Peg, we have used the VWA tool for the abundance analysis, and we refer to Sect. 7 for further information on atmosphere models, atomic data information, $\log(gf)$ adjustments etc. One important difference is, however, that for BW Aqr disentangling is not possible, and the analysis is therefore based on double-lined spectra.

Table A.1. Log of the FEROS observations of BW Aqr.

HJD−2 400 000[a]	phase	t_{exp} [b]	S/N[c]
51393.82092	0.1290	3600	140
51394.70920	0.2612	3600	200

[a] Refers to mid-exposure
[b] Exposure time in seconds
[c] Signal-to-noise ratio measured around 6070 Å

Table A.2. Astrophysical data adopted for the abundance analysis of BW Aqr.

	Primary	Secondary
$T_{\rm eff}$ (K)	6300	6225
$\log g$ (cgs)	4.075	3.981
$v \sin i$ (km s^{-1})	14.0	14.0
v_{micro} (km s^{-1})	1.70	1.50

The effective temperatures, surface gravities, rotational velocities, and microturbulence velocities listed in Table A.2 were adopted. The temperatures were determined by requiring that Fe I abundances were independent of line excitation potentials. They are slightly lower than determined by Clausen (1991), who obtained 6450 ± 100 K (primary) and 6350 ± 100 K (secondary). However, new and better (unpublished) *uvby* photometry for BW Aqr and the calibration by Holmberg et al. (2007) lead to 100 K lower values, assuming a reddening of $E(b-y) = 0.03$. Microturbulence velocities were tuned until Fe I abundances are independent of line equivalent widths.

The abundances derived from all useful lines in both spectra are presented in Table A.3. The equivalent widths measured in the two double-lined spectra are listed in Tables 16 (primary) and 17 (secondary), which will only be available in electronic form. Comparing the results from the two spectra, we find that they agree within 0.05 dex. We have only included lines with *measured* equivalent widths above 10 mÅ and below 45 mÅ (primary) and 55 mÅ (secondary). The lines are diluted by factors of about 2.2 (primary) and 1.8 (secondary), meaning that lines with *intrinsic* strengths above 100 mÅ are excluded. The [Fe/H] results for the two components differ by 0.06 dex, but for each component the results from Fe I and Fe II lines agree well. The mean value for all measured Fe lines is [Fe/H] $= -0.07 \pm 0.01$ (rms of mean).

Changing the model temperatures by ±100 K modifies [Fe/H] from the Fe I lines by about ±0.10 dex, whereas almost no effect is seen for the Fe II lines. If 0.30 km s^{-1} higher microturbulence velocities are adopted, [Fe/H] decreases by about 0.05 dex for both neutral and ionized lines. Taking these contributions to the uncertainties into account, we adopt [Fe/H] $= -0.07 \pm 0.11$ for BW Aqr. Similar abundances are obtained for the few other ions listed in Table A.3.

List of Objects

Table A.3. Abundances ([El./H]) for the primary and secondary components of BW Aqr determined from the two FEROS spectra.

	Primary			Secondary		
Ion	[El./H]	rms	N_t/N_l	[El./H]	rms	N_t/N_l
Si I	−0.12	0.02	3/2	−0.05	0.12	13/7
Ca I	−0.18	0.13	3/2	−0.00	0.09	7/4
Sc II				−0.08	0.08	3/2
Ti I	−0.02	0.09	3/2			
Cr I	−0.12	0.17	4/2	−0.04	0.12	5/4
Fe I	−0.11	0.16	65/41	−0.05	0.11	80/50
Fe II	−0.09	0.18	14/8	−0.03	0.11	14/8
Ni I	−0.05	0.14	18/11	−0.12	0.10	15/10

NOTE: N_t is the total number of lines used per ion, and N_l is the number of different lines used per ion. Ions with at least 3 lines measured are included.

'BK Peg' on page 2
'HD 222249' on page 3
'HD 222391' on page 3
'HD 223323' on page 3
'V442 Cyg' on page 11
'FS Mon' on page 11
'HD 71636' on page 11
'V1130 Tau' on page 11
'AD Boo' on page 11
'VZ Hya' on page 11
'V570 Per' on page 11